

# An Autocorrelator-Interferometer used to Determine the Pulse Width of a Pulsed Laser used in Two-Photon Endoscopy

By

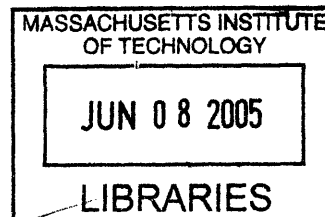
Nicholas A. Baksh

SUBMITTED TO THE DEPARTMENT OF MECHANICAL ENGINEERING IN  
PARTIAL FULFILLMENT OF THE REQUIREMENTS FOR THE DEGREE OF

BACHELOR OF SCIENCE IN MECHANICAL ENGINEERING  
AT THE  
MASSACHUSETTS INSTITUTE OF TECHNOLOGY

May 2005

[June 2005]



Signature of Author: \_\_\_\_\_  
Department of Mechanical Engineering  
May 18, 2005

Certified by: \_\_\_\_\_  
Peter So  
Professor of Mechanical Engineering  
Thesis Supervisor

Accepted by: \_\_\_\_\_  
Ernest G. Cravalho  
Professor of Mechanical Engineering  
Department Head for Mechanical Engineering

ARCHIVES

# **An Autocorrelator-Interferometer used to Determine the Pulse Width of a Pulsed Laser used in Two-Photon Endoscopy**

**By**

**Nicholas A. Baksh**

**Submitted to the Department of Mechanical Engineering  
on May 18, 2005 in Partial Fulfillment of the  
Requirements for the Degree of Bachelor in Science in  
Mechanical Engineering**

## **ABSTRACT**

An autocorrelator-interferometer was designed to correctly assess the pulse width of pulse laser used in two photon endoscopy. The path length of the light was altered using a retro-reflecting corner cube attached to a 6880 galvanometer optical scanner controlled by a 671 series micro-max controller (both products by Cambridge Technologies Inc.) The scanner was selected due to its ability to traverse very small rotations with a constant angular velocity, thereby reducing any non-linearities (with respect to time) in the autocorrelation. The projected results of this autocorrelator suggest it can be used to analyze electromagnetic waves with pulses on the order of a couple picoseconds, however, due to an imbalance of the scanner's shaft, the device was broken before any tests could be performed. A preliminary analysis suggests that a circular shaft attachment could be used to prevent this problem in the future.

Thesis Supervisor: Peter So  
Title: Professor of Mechanical Engineering

## Table of Contents

Section	Page Number
<b>I Introduction</b>	<b>1</b>
<b>II Background and Theory</b>	<b>2</b>
<b>III Materials and Methods</b>	<b>3</b>
<b>IV Results and Future Work</b>	<b>7</b>
<b>V Conclusion and Discussions</b>	<b>8</b>
<b>VI References</b>	<b>9</b>

## List of Figures

Figure	Page Number
<b>I Schematic of Optical Setup</b>	<b>2</b>
<b>II The 6880 Optical Scanner</b>	<b>4</b>
<b>III The 671 Micro-max Controller</b>	<b>4</b>
<b>IV Idealized Motor Shaft and Circuit For the 6880 Optical Scanner</b>	<b>5</b>
<b>V Power Supply and Enclosure</b>	<b>6</b>
<b>VI Optical Setup</b>	<b>7</b>
<b>VII Schematic of Balanced Shaft Attachment</b>	<b>8</b>
<b>VIII Predicted Results</b>	<b>8</b>
<b>IX Geometric Overview of Retro-reflecting Corner Cube</b>	<b>10</b>
<b>X Idealized Motor Shaft and Circuit For the 6880 Optical Scanner</b>	<b>11</b>
<b>XI Idealized Motor Shaft and Circuit For the 6880 Optical Scanner (No Transfer Functions)</b>	<b>13</b>

## 1.0 Introduction

Endoscopy is a commonly used clinical diagnosis method for internal organs. Typically, endoscopy only measures organ surface morphology with image resolution on the order of ten microns. Consequently, endoscopy does not provide cellular level information that is provided by histopathology where cellular layers and intracellular organs can be visualized to provide diagnostic information. Recent advances in this field have resulted in the development of novel 3D imaging endoscopes with subcellular resolution that can image specific cell layers down to a depth of a few hundred microns. Two forms of 3D, high resolution endoscopes have been developed based on one-photon and two-photon confocal principles.

One-photon confocal endoscopes can be implemented in two ways: the reflected light mode and the fluorescence mode. Reflected light confocal endoscopes measure the optical signal reflected from tissue refractive index heterogeneities. Reflected light confocal endoscopes use low power infrared light that is absorbed minimally by tissues and have penetration of a few hundred microns. One-photon fluorescence endoscope is less successful. Due to tissue constituents which have excitation spectra in the ultra-violet and blue, green spectral range, one-photon fluorescence excitation has short tissue penetration depth (about 100 microns) and often produces tissue photodamage.

While reflected light confocal endoscopes provide useful morphological signals from tissues, tissue biochemistry cannot be assayed using this method. A fluorescence confocal endoscope can assay tissue biochemistry, but cells become photodamaged and penetration depth limit is very small. Thus, our group focuses on the development of two-photon endoscopes. The two-photon endoscope is based on a non-linear excitation of fluorophores in tissues. Fluorophores can be excited in the infrared wavelength range by simultaneous absorption of two photons. Since this photo-interaction occurs only in the focal volume, minimal photodamage is induced in the tissue. Further, since infrared light is used similar to reflected light confocal endoscope, the two-photon system also has a large penetration depth (relatively).

Two photon endoscopy enables a safer tissue diagnostic method than one photon fluorescence endoscopy. However, it is still a relatively new technique and many problems have to be overcome before its clinical application. This thesis focuses on one of these obstacles. Two-photon excitation is a non-linear optical process and requires the use of high intensity excitation light source. Typically, pulsed infrared laser light source with pulse width on the order of 100 femtoseconds is used to maximize excitation efficiency. However, these laser pulses can be altered slightly as it passes through the optics in the instrument as well as the specimen. One important alteration corresponds to an increase in the pulse width of the laser caused by group velocity dispersion in high refractive index material and may result from scattering of light in the tissue. Without knowing the exact pulse width of the laser in the sample, we can not determine the energy being transferred to the sample.

It has been suggested that an autocorrelation measurement of the pulsed laser beam may be implemented to measure the pulse width of laser light in biological specimens. The autocorrelation function yields the correlation of the wave with itself. Generally, the autocorrelation function is used to determine if there is any lag or phase shift between two identical waves, however, the autocorrelation graph would also provide the pulse width of the laser beam. My thesis describes the design and initial construction of an autocorrelator that is compatible with the measurement of laser pulse width in tissue specimens through a two-photon microscope or endoscope.

## 2.0 Background and Theory

The interferometer-autocorrelator exploits the interference pattern produced by a standard interferometer to yield the autocorrelation of an electromagnetic wave. The standard interferometer setup employed is given in figure 1.

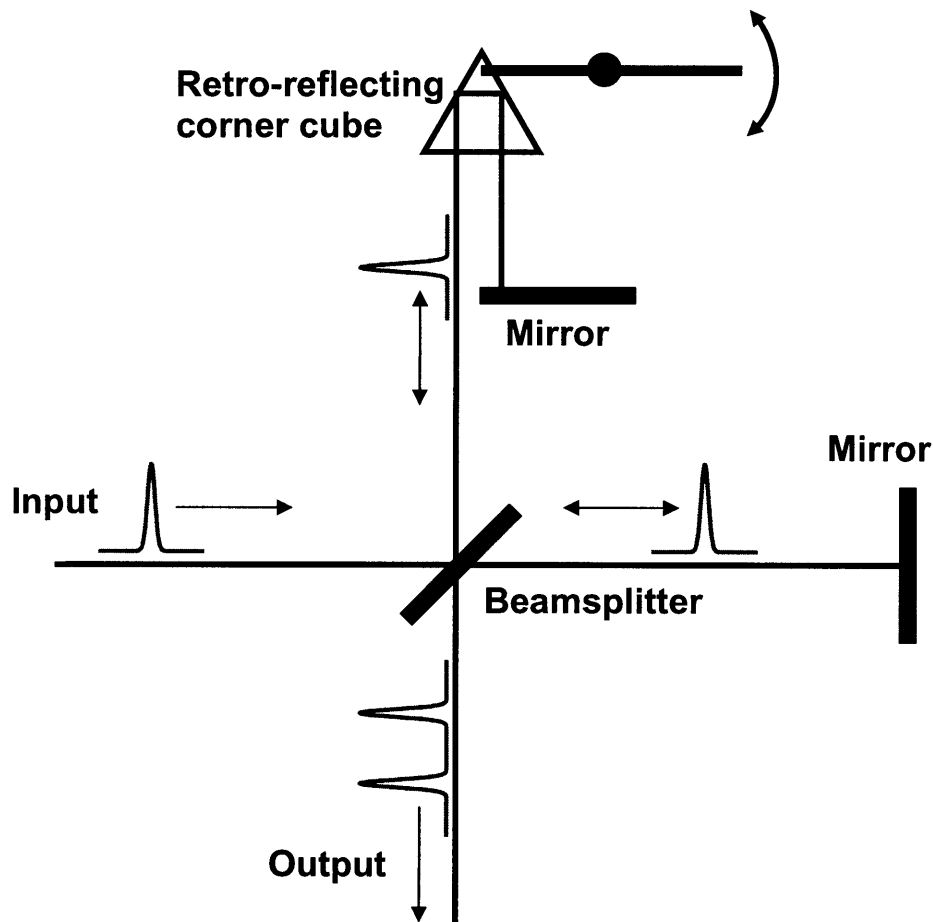


Figure 1: The Optical Setup for the Interferometer-Autocorrelator

The input, an electromagnetic wave, is split into two equal waves at the beam splitter and then recombined at this same point after each wave has traversed its respective path. One wave travels a fixed distance  $X$  (to the mirror and back), while the other beam travels a variable distance controlled by the angle of the retro-reflecting corner cube. As the cube is rotated, the path length is altered. The length is varied slowly, producing a maximum length change of at least one wavelength. Thus, as the angle and path length are changed, the waves are combining with different interference relationships at the beam splitter. These various interference relationships are recorded as the output by a photodiode. The continuous display of these interference patterns is the autocorrelation of the electromagnetic wave.

### **3.0 Materials and Procedure**

Essentially, the schematic depicted in figure 1 is used to produce the autocorrelation. A model 6880 galvanometer scanner along with its companion control board, a high accuracy 671 series Micromax controller, is used to rotate the corner cube refractor, thereby, changing the path length of the laser. The output is recorded by a photodiode and displayed on a monitor.

#### *3.1 Path Length Calculation*

The maximum pulse width that we intended to measure is about 20 picoseconds corresponding to a path difference of about 6mm in the autocorrelator. The geometry predicts that a  $4^\circ$  rotation of the retro-reflecting cube will produce a path length change of 6.813 mm; which is adequate for our measurement (see Appendix A for geometric picture and actual calculation). (Take care to note that these calculations were done assuming the mirror was attached to a bar at a distance 5cm from the scanner shaft. The picture of the bar and scanner is shown in figure 2.)

#### *3.2 The Scanner and Control Board*

A model 6880 galvanometer optical scanner from Cambridge Technologies Inc. was utilized to control the angle at which the retro-reflecting cube was held. As shown in figure 2, the scanner shaft was attached to an aluminum bar with the mirror attached 5cm away from the shaft. The bar was used to minimize the angle required to change the path length the designated amount. The scanner operates at a relationship of 1 degree per 0.5 mV and has a ten micro-radian sensitivity.

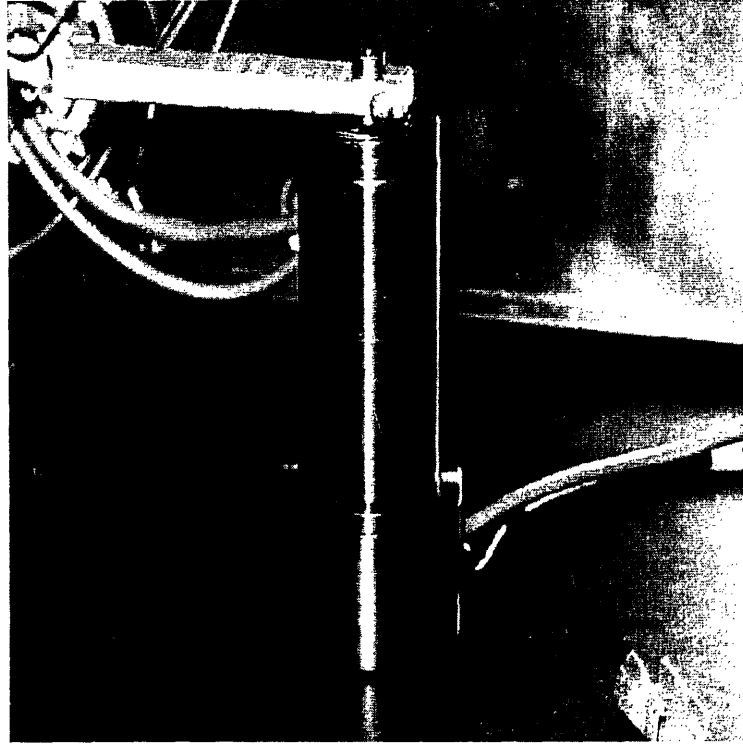


Figure 2: The 6880 Galvanometer Optical Scanner by Cambridge Technologies; slightly modified to incorporate a small aluminum bar.

The optical scanner was controlled with a MicroMax 671 Series controller from Cambridge Technologies Inc. The motherboard and its schematic are given in figure 3.

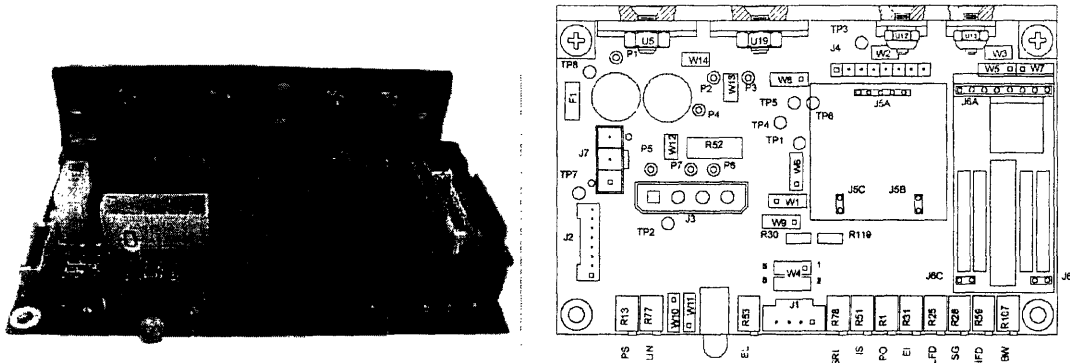


Figure 3: The actual micromax 671 controller by Cambridge Technologies Inc. (on the left) and its schematic (on the right). Briefly, J1 is the signal input, J2 and J7 are the scanner connection ports, and J3 is the power input. You may consult the actual manual for more of these details.

### 3.3 Heat Sinking

Heat sinks were required for both the scanner and the control board. Both heat sinks were made from aluminum and built to the specifications outlined in each manual assuming that the maximum power supply was 112 W. Further, two fans were mounted to the

enclosure to improve ventilation and convective heat transfer. The heatsinks and the fans can be seen in figures 5 and 6.

### 3.4 Power Supply

The power supply was evaluated differently than suggested by the manuals since the estimate derived in that manner was extremely large (on the order of 200 W). Instead, the scanner was modeled as an idealized rotor circuit and shaft as pictured in figure 4. This, in turn, yields the following transfer function:

$$\theta/V = K / \{s*[(Js+b)(Ls+R) + K^2]\} \quad (1)$$

where  $\theta$  is the angle imposed on the shaft,  $V$  is the voltage,  $K$  is the motor constant,  $s$  is the Laplace value,  $J$  is the moment of inertia of the load on the shaft,  $R$  is the resistance,  $L$  is the inductance, and  $b$  is the damping coefficient. All the relevant constants can be found in the manual. It was found that two 28 volt, 2 amp power supplies would not only power the system, but be more than adequate to account for any losses in the system. For a more detailed derivation of the transfer function, consult appendix B and for an approach which does not use transfer functions, please consult appendix C.

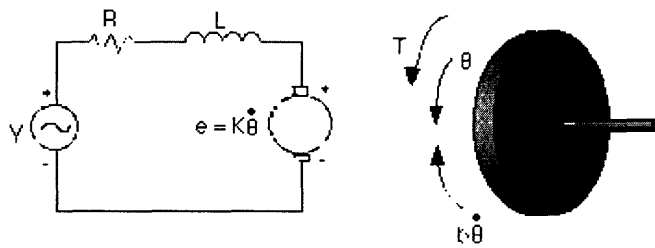


**Figure 4: Idealized rotor circuit and shaft.**

### 3.5 Enclosure

An enclosure was used to house the motherboard and power supplies. Fans were installed along its sides to help increase the convective heat transfer. The enclosure is pictured in figure 5.

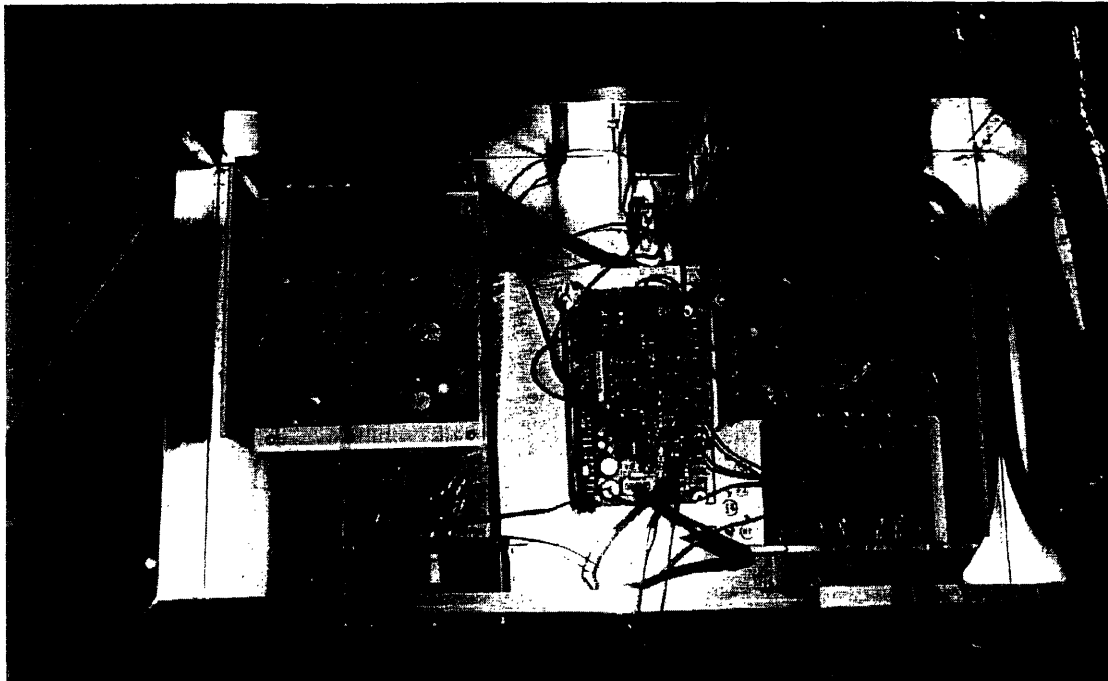


**Figure 5: The enclosure with the two power supplies on the sides wired to the 671 controller in the middle. The power supplies are wired at +/- 28 volts.**

### *3.6 The Optical Setup*

The schematic diagram of the optical setup is given in figure 1 and described in section 2.0. Figure 6 depicts the actual setup employed.

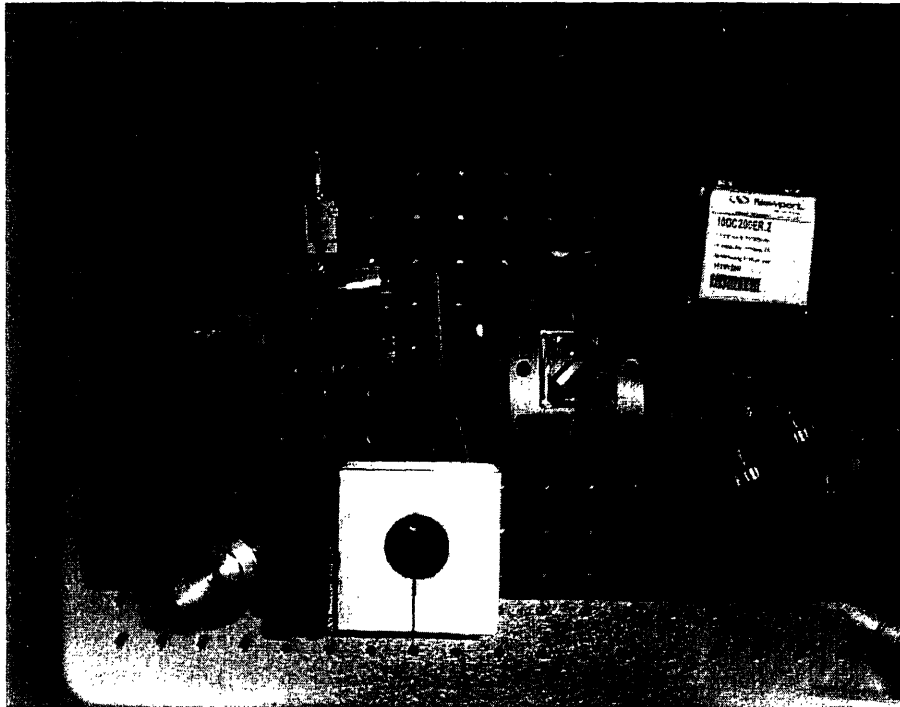


Figure 6: The optical setup employed. The laser is split at the beam splitter into two equal waves, each traverse their respective distances before recombining at the beam splitter and being recorded at the photosensor.

#### 4.0 Results/ Future Work

Unfortunately, due to a minor tuning error, the control board for the scanner malfunctioned. As a result, the scanner became unresponsive to any input signal. It was determined that the scanner can not be tuned to handle the torque imposed by the attached mirror and shaft. Even though the load and the moment of the attachment are less than the maximum values suggested by the manual, the imbalance brought about by the shape of the bar makes tuning difficult and dangerous to the board. As a result, in the future, an evenly balanced attachment should be used. A quick fix could be simply a circular disc with a mirror and a balancing mass attached as schematically drawn in figure 7.

A sample of predicted results can be seen in figure 8.

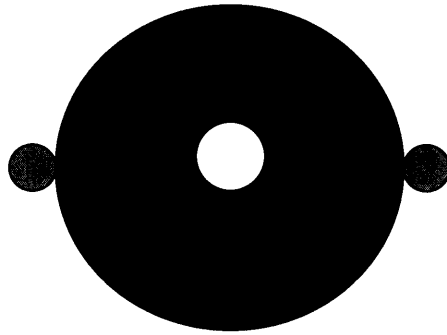


Figure 7: Schematic of a balanced shaft attachment for the 6880 scanner.

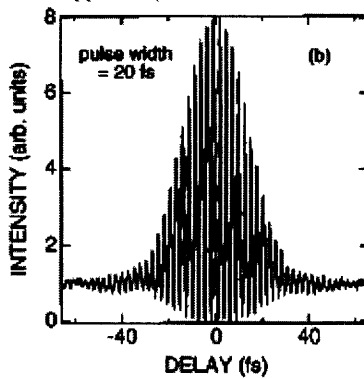


Figure 8: Predicted autocorrelation for a laser with and FWHM of about 20fs. This picture was taken from the Riffe and Sabbah source (Source 1).

## 5.0 Conclusion/Discussion

Similar type of interferometer-autocorrelator has been successfully implemented and used to establish the pulse width of picosecond and femtosecond laser pulses (Riffe). However, many designs have failed to produce purely linear relationships between the phase (angle) and the lag (time) because they fail to alter the path length of the laser at a constant rate. These designs require post data acquisition correction to account for this non-linearity. The model 6880 galvanometer scanner promises precise, high accuracy movements at a constant rate. If a balanced bar attachment can be designed accurately (as in figure 7), the galvanometer could enable the interferometer-autocorrelator to produce the linear relationship. If the circular disc proposed fails and no other design can be established, a larger galvanometer can be used to elicit the same result, the drawback being the increased price.

Nonetheless, the interferometer-autocorrelator enables high accuracy assessment of a laser's pulse width. With this energy value, lasers can be used to image specimens as described in section 1.0.

## **6.0 References**

D. M. Riffe and A. J. Sabbah. A compact rotating-mirror autocorrelator design for femtosecond and picosecond laser pulses. *Physics Department, Utah State University, Logan, Utah 84322-4415*. 15 June 1998.

## Appendix A: Path Length Calculation

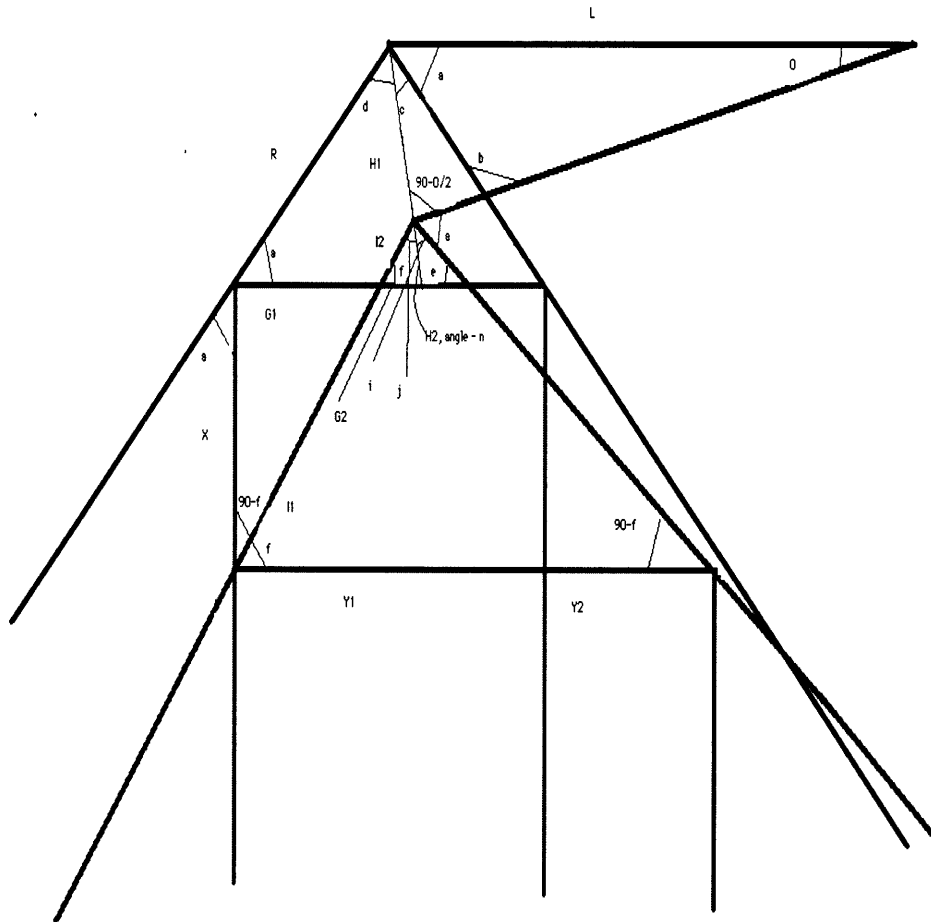


**Figure 9: Geometric overview of the retro-reflecting corner cube with an angle imposed.**

From this diagram, the resultant path length change from the angle change can be solved for analytically if  $L$ ,  $R$ ,  $\theta$  and  $\alpha$  are given. In the experiment,  $L$  was set to 5cm,  $R$  was set to 1cm and both angles were set to  $45^\circ$ .

## Appendix B: Derivation of Transfer Function for Scanner

The model 6880 Galvanometer Optical Scanner by Cambridge Technology, Inc is capable of producing fast, accurate angular displacements. Ultimately, the device imposes a torque on the exposed cylindrical shaft in response to a current stimulus. The operations are very similar to a simple DC motor, and thus, for a first order approximation, can be modeled as such. Pictured below are two schematics, a simple DC motor and the ideal generalization of the rotor circuit which controls it.

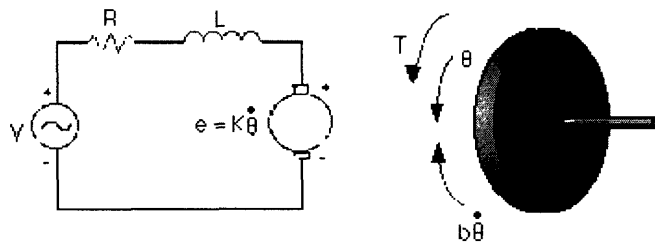


**Figure 10: Idealized Rotor Circuit and Shaft**

The motor torque,  $T$ , is related to the current  $i$ , by a constant factor  $K_t$ . Similarly, the back emf,  $e$ , is also a function of a constant, namely  $K_e$ , however  $e$  is related to the angular velocity by this constant.

$$T = K_t i \quad (1)$$

$$e = K_e \omega \quad (2)$$

In most cases, the  $K_t$  (armature constant) is roughly equal to  $K_e$  (motor constant) (thus, hereafter both will be referred to as  $K$ ).

Applying Newton's and Krichoff's laws to the figures yields the following equations:

$$J \ddot{\theta} + b \dot{\theta} = K i \quad (3)$$

$$L \cdot i' + Ri = V - K\theta' \quad (4)$$

where the substitution  $\omega = \theta'$  has been applied. Also note that  $J$  is the moment of inertia,  $b$  is the damping coefficient,  $i$  is the current,  $L$  is the inductance in the circuit,  $R$  is the resistance, and  $V$  is the voltage. Lastly, take care to realize that  $\theta$  is the angular displacement,  $\theta'$  is the angular velocity, and  $\theta''$  is the angular acceleration.

Using Laplace transforms, the equations can be written in terms of  $s$ .

$$S(Js+b) \theta(s) = KI(s) \quad (5)$$

$$(Ls+R)I(s) = V - Ks \theta(s) \quad (6)$$

Eliminating  $I(s)$  yields the following transfer function, where the angular velocity is the output and the voltage is an input.

$$\theta'/V = K / [(Js+b)(Ls+R) + K^2] \quad (7)$$

However, position is the desired output. Integrating the angular velocity (dividing the transfer function by  $s$ ) yields the final results with position as the output.

$$\theta/V = K / \{s^*[(Js+b)(Ls+R) + K^2]\} \quad (8)$$

Lastly, it should be clarified that the differential equations in 3 and 4 can be reduced to a single second order homogenous differential equation which can then be solved numerically without the use of Laplace transforms. The analysis to obtain the homogenous equation is given in appendix A through slightly different example.

## Appendix C: Modeling of Scanner without Transfer Functions

The model 6880 Galvanometer Optical Scanner by Cambridge Technology, Inc is capable of producing fast, accurate angular displacements. Ultimately, the device imposes a torque on the exposed cylindrical shaft in response to a current stimulus. The operations are very similar to a simple DC motor, and thus, for a first order approximation, can be modeled as such. Pictured below are two schematics, a simple DC motor and the ideal generalization of the rotor circuit.

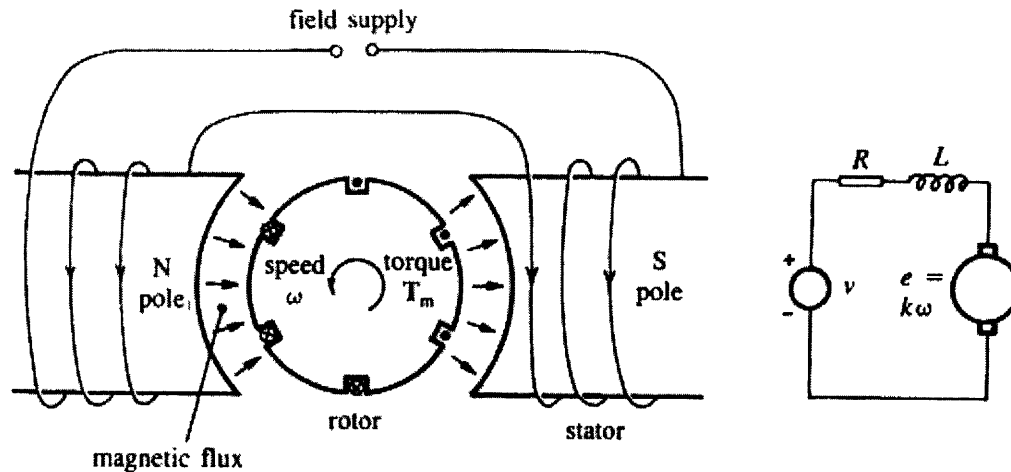


**Figure 11: Schematic diagram of a d.c. motor and the electric diagram of the rotor circuit.**

The final torque experienced by the system is the difference between the torque applied by the motor and the torque imposed by the load (of the entire shaft being rotated). The applied torque is simply proportional to the current while the imposed torque load is a combination of Coulomb friction and a spring constant (which compensates for the damping effect noticed when an angular acceleration is applied to the scanner shaft). Applying these values to the equilibrium condition produces the following equation of motion,

$$I * \theta'' = K_m * i - \tau_{cf} - K_s * \omega \quad (1)$$

Where  $I$  is the moment of inertia,  $\theta''$  is the second derivative of the angular displacement,  $K_m$  is motor constant,  $i$  is the current,  $\tau_{cf}$  is the torque due to Coulomb Friction,  $K_s$  is the damping constant, and  $\omega$  is the angular velocity.

Applying a similar control analysis to the rotor circuit, we find that

$$L * i' = v - R*i - K_g * \omega \quad (2)$$

Where L is the inductance, v is the potential difference, R is resistance, and  $K_g$  is the circuit back emf constant.

The first differential equation can be separated by noting that  $\theta' = \omega$ . With this substitution and some algebraic manipulation, equation 1 can be expressed as

$$I / (X - K_s * \omega) * d\omega = 1 dt \quad (3)$$

Where  $X = K_m * i - \tau_{cf}$ . Evaluating this integral yields

$$t(\omega) = - I/K_s * \ln (-K_s * \omega + X) \quad (4)$$

or with some manipulation,

$$\omega(t) = [\exp(-K_s * t/I) - X] / K_s \quad (5)$$

This value can be substituted into the second differential equation given above to cancel out the  $\omega$  variable yielding the following homogenous differential equation:

$$L * i' = v - R*i - K_g * (\exp(At)/K_s - B) \quad (6)$$

Where  $A = - K_s/I$  and  $B = X/K_s$ . This solution can then be solved numerically for the feasible voltage/current pairs in the circuit. These values can then be used to establish  $\omega$  and then  $\theta$ .